

Non-invasive imaging methods in cephalopod research

R. Hoffmann et al.

Non-invasive imaging methods applied to neo- and paleontological cephalopod research

R. Hoffmann¹, J. A. Schultz², R. Schellhorn², E. Rybacki³, H. Keupp⁴,
S. R. Gerden¹, R. Lemanis¹, and S. Zachow⁵

¹Institut für Geologie, Mineralogie und Geophysik, Ruhr Universität Bochum, Universitätsstrasse 150, 44801 Bochum, Germany

²Steinmann-Institut für Geologie, Mineralogie und Paläontologie, Rheinische Friedrich-Wilhelms-Universität Bonn, Nussallee 8, 53115 Bonn, Germany

³Helmholtz-Zentrum Potsdam, Deutsches GeoForschungsZentrum GFZ Sektion 3.2, Geomechanik und Rheologie, Telegrafenberg, D 429, 14473 Potsdam, Germany

⁴Institut für Geologische Wissenschaften, Fachrichtung Paläontologie, Freie Universität Berlin, Malteserstrasse 74–100, 12249 Berlin, Germany

⁵Zuse Institut Berlin, Takustrasse 7, 14195 Berlin, Germany

Received: 28 October 2013 – Accepted: 13 November 2013 – Published: 29 November 2013

Correspondence to: R. Hoffmann (rene.hoffmann@rub.de)

Published by Copernicus Publications on behalf of the European Geosciences Union.

Title Page

Abstract

Introduction

Conclusions

References

Tables

Figures

◀

▶

◀

▶

Back

Close

Full Screen / Esc

Printer-friendly Version

Interactive Discussion



Abstract

Several non-invasive methods are common practice in natural sciences today. Here we present how they can be applied and contribute to current topics in cephalopod (paleo-) biology. Different methods will be compared in terms of time necessary to acquire the data, amount of data, accuracy/resolution, minimum-maximum size of objects that can be studied, of the degree of post-processing needed and availability. Main application of the methods is seen in morphometry and volumetry of cephalopod shells in order to improve our understanding of diversity and disparity, functional morphology and biology of extinct and extant cephalopods.

1 Introduction

During the last decade non-invasive diagnostics became increasingly important for paleontological research. The analysis of shapes of fossil hard parts, either fully or partially preserved within the surrounding rocks, requires imaging methods that are primarily used in non-destructive testing. The preservation of the specimen is of main importance using these methods since former techniques used destructive methods leading to the loss of the specimen or parts of the specimen. Enhanced tomographic imaging techniques enable a view inside of solid objects with astonishing spatial resolution. Typical tasks for the reconstruction of structures from tomographic image data are digital image processing (like filtering, enhancement), segmentation (e.g., classification), and geometry processing.

The oldest record of the application of non-invasive methods in the field of cephalopod-research dates back to the publication of Lehmann (1932). By using x-rays Lehmann (1932) produced stereo-images of a 3-D impression of the internal structures of a Lower Jurassic ammonite. A few years earlier Sollas (1904) invented a method using serial sections which allowed the visualization of internal structures of fossils. This approach has formed the basis of modern grinding tomography (e.g.,

BGD

10, 18803–18851, 2013

Non-invasive imaging methods in cephalopod research

R. Hoffmann et al.

Title Page

Abstract

Introduction

Conclusions

References

Tables

Figures



Back

Close

Full Screen / Esc

Printer-friendly Version

Interactive Discussion



BGD

10, 18803–18851, 2013

**Non-invasive imaging
methods in
cephalopod research**

R. Hoffmann et al.

Title Page

Abstract

Introduction

Conclusions

References

Tables

Figures



Back

Close

Full Screen / Esc

Printer-friendly Version

Interactive Discussion



Pascual-Cebrian et al., 2013). Much has been improved since the earliest attempts, invasive or not, for 3-D reconstructions of fossils and their internal structures (Sollas and Sollas, 1914; Tipper, 1976; Luo and Ketten, 1991; Herbert et al., 1995; Hurum, 1996; Stock, 2006; Tafforeau et al., 2006; Sutton et al., 2001; Hoffmann and Zachow, 2011; Falkingham, 2012). Advantages and disadvantages of non-invasive methods (surface scanning, computed tomography, magnetic resonance tomography) tested by the authors are discussed below.

Advantages of the non-invasive approach are: external and/or internal structures of specimens can be studied in great detail while the specimen itself remains untouched (Fig. 1), scan-data can be shared within the scientific community, used for a virtual visit of museum's collections (e.g., <http://www.3d-fossils.ac.uk/home.html>), to maintain a record of type material that may later be destroyed or lost in the future or can be stored for later studies to solve new questions. A clear advantage for future work is the possibility to store and share the CT-data and make them available for subsequent studies of other researchers. Rare fossils (e.g., holotype material) can be duplicated as 3-D-prints and send to scientists all over the world or used for lectures (Rahman et al., 2012), exhibitions and outreach programs. Single pieces of a broken specimen can be scanned separately, merged digitally – as shown by Hoffmann (2010) for an Upper Cretaceous hollow preserved ammonite – and printed in one piece afterwards (Fig. 1b). Multiplanar reconstructions (MPR, Fig. 1a), surface- and volume renderings (Fig. 3b) can also be applied to the datasets. Presentations animations and instructive movies can be created. Finally, accurate surface models can be derived from these methods and be used for advanced functional analyses such as finite element analysis, computational fluid dynamics and multibody dynamic analysis (Anderson et al., 2012). One main goal for future research should be the establishment of a 3-D shape database for ammonoids, comparable to the gen bank of biologists.

We chose cephalopods as ideal candidates for this non-invasive method study because of their longevity, high abundances and wide distribution during earth's history, their meaning for biostratigraphy due to high evolutionary rates, importance for tracing

BGD

10, 18803–18851, 2013

Non-invasive imaging
methods in
cephalopod research

R. Hoffmann et al.

Title Page

Abstract

Introduction

Conclusions

References

Tables

Figures



Back

Close

Full Screen / Esc

Printer-friendly Version

Interactive Discussion



evolutionary mechanisms and their complex internal structure and its possible function which was under debate for centuries. Besides measuring distances the main challenge here is to test whether the ammonoids – a group that appeared during the Devonian and went extinct at the Cretaceous-Paleogene event – could swim or not. In order to answer this question we performed the first test with the shells of the recent *Nautilus* and *Spirula* and calculated the buoyancy values for each. For both species it is well known that they were able to swim freely in the water column. Non-invasive methods therefore offer a good option for 2-D and 3-D measurements of cephalopod shells and will contribute to the quantitative morphological approach taking intraspecific variability of species into account (Hoffmann et al., 2012).

Due to their accretionary growth mollusks keep their whole ontogeny preserved within their shells. 2-D measurements of distances and their ontogenetic changes (ontogenetic trajectories) with a higher resolution (from 45° down to 1°) compared to the grinding/cutting approach (180° or 90°) will contribute to our understanding of the morpho-species concept (diversity vs. disparity). First 2-D measurements were performed on the micro-CT images of the extant *Nautilus* and *Spirula* and afterwards on the micro-CT images of fossil ammonites following the key of description for ammonoid conchs of Korn (2010). Due to the advantages of some of the non-invasive methods we were able to add internal characters to the classical data (e.g., ammonitella length, septal angle, septal thickness profiles, septal spacing, diameter of the siphuncle at a certain conch diameter, relative position of the siphuncle, and conch wall thickness at a certain conch diameter). Only after segmentation the CT-data can be analyzed for ontogenetic changes of volumes (chambers, shell) and finally a buoyancy calculation. The obtained 3-D surface models of ammonoids and other cephalopods can subsequently be transferred into finite element software (e.g., hypermesh to apply stress and strain analysis) but this is beyond the scope of this contribution. To the best of our knowledge there is so far no study available comparing different non-invasive methods and their potential to solve open questions in cephalopod research.

2 Material

For comparison of the different methods we examined shells of two extant cephalopods (e.g., the deep sea squid *Spirula spirula* from the Canary Island with a diameter of 1.6 cm (coll. R. Hoffmann, SsCI_01), and a 17 cm diameter *Nautilus pompilius* from the Philippines (coll. R. Hoffmann, NpPh_01)). As representatives of the extinct ammonoids we examined an *Eleganticeras* sp. from the Lower Jurassic of Germany (coll. R. Hoffmann, EIGr_01), a giant *Lobolytoceras costellatum* from the Upper Jurassic (Oxfordian) of Madagascar (coll. H. Keupp, MAn-3059, 61.5 cm in diameter), three juvenile Upper Jurassic (Callovian) ammonites (?*Cadoceras* sp.) from the Kostroma region of Russia with a diameter between 2 and 5 mm in diameter (coll. R. Hoffmann, CaKr_01, CaKr_02, CaKr_03), a *Gaudryceras* sp. about 5 cm in diameter, scanned with the surrounding concretion of about 20 cm (Fig. 1b) from the Upper Cretaceous (Maastrichtian) of Kamchatka (coll. Y. Shigeta, Tokyo, without invent-nr.) – the latter two are preserved in nearly hollow condition, one median section of *Argonauticeras* sp. of 9.5 cm diameter, from the Lower Cretaceous (Albian) from Madagascar (coll. R. Hoffmann, ArMa_01). A single pathological rostrum of the belemnite *Hibolithes jaculoides* (coll. H Keupp, PB251) from the Lower Cretaceous (Hauterivian) of Heligoland (Germany) and one calcite crystal were also examined.

3 Methods

3.1 Surface scanning

A variety of manufacturers provide products to digitize objects of different sizes and materials in a broad spectrum of resolutions and different price segments. A low cost solution to produce surface scans is, for instance, provided by DAVID[®], but other brands come up with more expensive products and more capabilities (e.g., STEINBICHLER[®], BREUCKMANN[®]), using other set ups and technologies being mo-

BGD

10, 18803–18851, 2013

Non-invasive imaging
methods in
cephalopod research

R. Hoffmann et al.

Title Page

Abstract

Introduction

Conclusions

References

Tables

Figures



Back

Close

Full Screen / Esc

Printer-friendly Version

Interactive Discussion



holes and detect them with the camera at the same time. This leads to missing data within the polygonal model causing holes in the surface mesh (Fig. 2). These holes can be closed during the data post processing (e.g., with PolyWorks[®]). With such post processing software the volume of any scanned object can be calculated. The accuracy of the calculated volume depends on the resolution and geometry but is independent of the chemical composition and therefore absorption properties or density of the object which plays an important role in computed tomography for instance (Table 1).

3.2 Computed tomography (CT)

Leading companies that produce medical CT scanners are NIKON[®], SIEMENS[®], PHILIPS[®] and General Electric[®] (GE[®]) among others. The resolution of CT-scanners extensively used in the field of medical care is between 2000 and 500 μm . A low cost solution is not available and a device can easily cost more than 500 k€ to date. The investigated giant ammonite (*Lobolytoceras costellatum*) has been scanned in 2007 at the Fachbereich Veterinärmedizin (Klinik und Poliklinik für kleine Haustiere), Freie Universität Berlin-Düppel using a medical CT-scanner from GE[®] with a resolution of 1 mm (Fig. 3). The objects of interest can easily be adjusted within the FOV by positioning them on a movable scanner table, which can be lifted up/down and moved back/forth. Further calibrations are not necessary because the x-ray source will rotate around the object(s). In comparison to surface scanning the reflectivity of the surface or organic matter are not problematic for x-ray scans (same for micro-CT, nano-CT, SR μ CT). Scan parameters are fixed in the associated scan programs. Due to the open construction of the relatively large medical CT-scanners a special room with x-ray absorption properties and low-vibrations is necessary. Medical CT-scanners are installed within a distinct room and cannot be easily moved to another locality. Contrary to the high costs for acquisition of a medical CT-scanner, they are widely distributed in different kinds of hospitals and therefore relatively easy to get access to. Scan time ranges between a few seconds and a few minutes depending on the size of the object of interest. The

BGD

10, 18803–18851, 2013

Non-invasive imaging methods in cephalopod research

R. Hoffmann et al.

Title Page

Abstract

Introduction

Conclusions

References

Tables

Figures

⏪

⏩

◀

▶

Back

Close

Full Screen / Esc

Printer-friendly Version

Interactive Discussion



reconstruction process (post-processing) can be completed in a few minutes due to the small amount of data which can be operated on a standard desktop PC. Open source software (e.g., ImageJ) is suitable for the post-processing work. The resulting images lack high precision due to a resolution of 500 μm . Depending on the available resolution the smallest objects should be generally not smaller than 1 cm. The upper limit of object size is around 180 cm in diameter which is six times larger compared to a micro-CT, but can be much longer. Dual-Energy scans are possible with medical CT-scanner devices using two x-ray sources and two detectors at the same time, the scanning speed is increased and of exceptional quality. Medical CT-scanners allow the detection of internal structures larger than 500 μm or the identification of fossils and their 3-D position within a larger rock sample. In addition several kinds of scan artifacts may occur in the reconstructed image due to limited x-ray flux or use of polychromatic radiation, finite resolution, discrete sampling and x-ray scatter, hindering a successful reconstruction of shapes (Davis and Elliott, 2006).

3.3 Micro-computed tomography (micro-CT)

The advantage of micro-CT technology, developed at the end of the 1980s, over conventional CTs is a significantly higher achievable resolution. Scanners are available from different companies (e.g., GE[®], Skyscan[®], FRAUNHOFER[®]) and are increasingly accessible in different scientific facilities with various fields of interests. A great number of micro-CT machines are chambered devices that do not need a special radiation protection area or an extra room with special lead coating for security as a protective lead coating is included in the chambered set-up. The workers using the micro-CT device normally need extra radiation security training, depending on the x-ray emission rate of the device. Due to the size (233cm \times 169cm \times 148cm) and mass (2900 kg) of such a device, most scanners are not easy to move. The desktop micro-CT device of Skyscan (now Bruker[®] micro-CT) is an exception in this category, as it is relatively small and mobile with a 100 kV x-ray tube and a maximum sample size of 20 mm. CT-

Non-invasive imaging methods in cephalopod research

R. Hoffmann et al.

Title Page

Abstract

Introduction

Conclusions

References

Tables

Figures



Back

Close

Full Screen / Esc

Printer-friendly Version

Interactive Discussion



BGD

10, 18803–18851, 2013

Non-invasive imaging methods in cephalopod research

R. Hoffmann et al.

[Title Page](#)
[Abstract](#)
[Introduction](#)
[Conclusions](#)
[References](#)
[Tables](#)
[Figures](#)
[Back](#)
[Close](#)
[Full Screen / Esc](#)
[Printer-friendly Version](#)
[Interactive Discussion](#)


MINI FRAUNHOFER[®] developed a portable micro-CT with the dimensions of 1 m × 1 m and a 90 kV x-ray tube. Maximum sample size is 35 mm × 35 mm × 25 mm with the highest possible resolution of 5 μm which is comparable to the portable Skyscan device. The maximum size of the objects to be scanned depends on the detector size, and the scanning chamber of the device. Objects larger than the detector maybe be scanned in parts and merged virtually afterwards. The detector of the phoenix|x-ray v|tome|x s 240 (GE[®]) housed in the Steinmann-Institut für Geologie, Mineralogie und Paläontologie (Universität Bonn, Germany) is 40 cm × 40 cm. The maximum object weight is 10 kg. The used device has two different tubes, a high-power nanofocus x-ray tube (180 kV, 15 W) and a microfocus tube (240 kV, 320 W). There are also micro-CTs available on the market independent from a chamber set up (for example the L products of GE[®]); here special rooms and technicians are necessary. Within a chambered device objects are mounted on a movable and rotatable computerized numerical control table (CNC table) and depending on the distance to the x-ray source the resolution of the scan changes. As a rule the closer you get, the higher is the resolution you can achieve. The resolution for the phoenix|x-ray v|tome|x s 240 ranges from 6–246 μm for the microfocus tube and down to 2 μm for the nanofocus tube. An advantage is that several small objects can be scanned at the same time with the same resolution. The utilization of high resolution scans allows the visualization of outer and inner structures (e.g., ornamentation, septa, of smaller dimensions and with increased precision compared to medical CT-scans) and the creating of detailed 3-D models of the scanned objects. For objects within or filled with matrix a successful segmentation depends on the state of preservation. A considerable difference of absorption properties between the structure/region of interest (fossil) and the surrounding matrix therefore is necessary. For segmentation, carbonaceous hard parts (aragonitic or calcitic) are inappropriate when preserved in carbonaceous matrix or filled with secondary calcite crystals/cement. The scan process is fully automatic, except for the adjustments before the start, and therefore the scanning with a micro-CT device is not time consuming. Disadvantages of a micro-CT device is the price (easily more than 500 k€ to date) and the need for ex-

tensive maintenance supplies (filaments, detector etc.). The huge datasets produced during one scan cannot be operated with a normal Desktop PC. Only a few software systems for 3-D image segmentation do exist that can handle large data sets and provide algorithms for the geometric reconstruction of multi-component structures. At Zuse Institute Berlin (ZIB) such a system is being developed that already provides algorithms to reconstruct geometry from large 3-D image data (ZIBAmira). The software is constantly improved at ZIB with respect to versatile research problems. Nevertheless, the post scan processing is mainly done with reconstruction software developed by the manufacturers of the micro-CT device that extracts the scan images from the raw data. Normally alignment optimization, beam-hardening and ring-artifact corrections are included in the reconstruction algorithm. As many devices produce different raw data formats the reconstruction after scanning elsewhere is problematic. Due to the well known sampling theorem (Nyquist, Shannon, Kotelnikov, Whittaker; see Marks II, 1991) the spatial resolution of the scanning system needs to be at least twice as high as the smallest structure that needs to be reconstructed from the image data. For example the highest resolution for a micro-CT is 2–5 μm the structure of interest needs to be at least 4–10 μm . The maximum resolution mode itself produces a very low signal to noise ratio (SNR) due to high sensitivity and sensor artifacts. That noise is degrading the image quality and hindering automatic segmentation algorithms to distinguish between the structures of interest and non-relevant structures and noise. Drews et al. (2008) conducted a comprehensive micro-CT study using a vertebral body. Several scans were performed with four different micro-CT systems of three manufacturers. They compared the quality of the images obtained from the tested devices against the results with the “golden standard” of the synchrotron tomography in order to find the best options for the geometric and volumetric analysis of bone tissue. For the visualization of smaller objects or structures, e.g., earliest ammonoid septa, protoconch, special scanning devices are required which can be operated with maximum resolution (e.g., phoenix nanotom[®]). Due to the wide distribution of micro-CTs at universities and other

BGD

10, 18803–18851, 2013

Non-invasive imaging methods in cephalopod research

R. Hoffmann et al.

Title Page

Abstract

Introduction

Conclusions

References

Tables

Figures



Back

Close

Full Screen / Esc

Printer-friendly Version

Interactive Discussion



institutions it is possible to get scans for 300 € up to 1000 €, the money is mainly used to cover the maintenance costs.

3.4 Nanofocus-computed tomography (nano-CT)

In 2006 GE[®] developed the phoenix nanotom[®] (nano-CT) a new tomograph device with improved resolution and contrast properties (Drews et al., 2008). Because of its weight of 1300 kg and the dimensions of 164 cm × 143 cm × 75 cm a suitable place has to be chosen with care as it is not easy to remove the device after installation. With its 180 kV/15 W high power nanofocus[®] x-ray tube and an improved detector using CCD or CMOS technology the nanotom[®] series was designed for material sciences but can also be used for geological and biological samples. It has a high precision rotation unit on which the scanned object can be easily mounted comparable to the procedure during micro-CT scanning. Like the micro-CT the nanotom[®] is a chambered device that includes lead coating and therefore does not need an extra room with special lead coating for security or a special radiation protection area. Maximum object size depends on the chamber- and detector-size and should not be larger than 150 mm × 120 mm and not heavier than 2 kg. Compared to a micro-CT from the same company scan artifacts are reduced and the contrast of the resulting grey-scale images is increased while the time effort stays the same. In addition, data acquisition needs half the time for the same image quality. Resolution was improved with the highest value at 0.5 μm but the detail-detectability lies at about 200–300 nm (Brunke et al., 2008). Thus, the dimension of the structure of interest suitable for a successful reconstruction is reduced to about 1–2 μm when compared to a micro-CT device. With the high power (15 W) high-absorption samples (high density materials) can be examined. In addition, the reconstruction of the scanned data is faster using a time optimized algorithm. Time necessary to scan a certain object depends on object size, scan-resolution, and numbers of images taken, rotational angle and time interval of rotation and may vary between several minutes to several hours. Due to the novelty of the technology a single company distributes the

BGD

10, 18803–18851, 2013

Non-invasive imaging methods in cephalopod research

R. Hoffmann et al.

Title Page

Abstract

Introduction

Conclusions

References

Tables

Figures



Back

Close

Full Screen / Esc

Printer-friendly Version

Interactive Discussion



depends on the main beam working stable. Therefore a huge setup (e.g., European Synchrotron Radiation Facility (ESRF) Grenoble, main beam lengths 844 m) with several technicians is necessary to induce the electrons. At least one additional technician is necessary on each beamline the user is working on. Scan time for one small object (5 mm) takes about 5–20 min, depending on the set up. But also larger objects can be scanned with high accuracy and high resolution. High resolution means in this case, that the resolution can be less than 1 μm (about 0.7 μm ; Tafforeau and Smith, 2013; Fig. 10). The great disadvantage of synchrotron technology is the huge amount of data that are produced during a single scan. The larger an object is, the larger the dataset gets (easily several terabytes) meaning short and long term data storage can be a potential problem. The data size elongates the reconstruction time afterwards to several days, depending on the number of specimens scanned. Since only a few synchrotron facilities are available worldwide so far, this method is rather hard to get access to, mainly depending on a scan proposal with an accurate project summary. A successful proposal is typically granted beam time for several days. Besides synchrotron micro computed tomography other methods are usually available at these facilities (e.g., phase contrast tomography or holotomography). For details the reader is referred to Stock (2006) and Tafforeau et al. (2006).

3.6 Magnetic Resonance Imaging (MRI)

Like CT-scanning MRI has its origin in medical sciences and clinical practice. Comparable to computed tomography it allows the study of skeletal hard parts and physiological processes in vivo. In contrast to CT-scanning MRI allows the differentiation between various types of soft tissues (organs). For fossil cephalopod material this method becomes interesting if a contrast agent like hydrogen was trapped within the skeletal material or an existing gap between the internal mould and the surrounding rock can be filled with a contrast agent. This gap usually represents the original place and morphology of the now dissolved shell. Under fortunate conditions (low porosity, no connected pore space) the gap filled with the agent allows the reconstruction of the shell.

Title Page

Abstract

Introduction

Conclusions

References

Tables

Figures



Back

Close

Full Screen / Esc

Printer-friendly Version

Interactive Discussion



There are a few companies distributing MRI scanners (e.g., SIEMENS[®], PHILIPS[®], GE[®], and BRUKER[®]). A low cost solution is not yet available. Portable MRI scanners are available but have no powerful polarizing magnet. These portables represent the cheapest solution but long scan times are required due to a low SNR. Nowadays lower limit of resolution for objects of about 1 cm is around 40 μm and for objects of 2–3 cm around 60–80 μm (A. Ziegler, personal communication, 2013). No special environment is needed to use the system. Sample size depends on the dimensions of the spectrometer used and the possibility to use the method itself depends on the presence of detectable contrast agent (e.g., water). Because the x-ray source will rotate around the objects, a special fixture of the object is not needed, but it should be positioned in a stable manner to avoid movements of the object during the scan. Post-processing and visualization of the images can be done using different software packages (e.g., ImageJ or Amira). The resulting file size depends on the size of the object and resolution but the data volume never exceeds the handling limits of a desktop PC. Due to relaxation constants and proton concentration the resolution of the MRI images is limited to 60–40 μm (Callaghan, 1991). Therefore, the reconstruction of structures of interest with dimensions smaller than 40 μm is not possible with this method. If no contrast agents are available this method cannot be applied. Another issue is the time consuming process, up to one week, to obtain the data which depends again on the proton concentration, the power of the used magnet and SNR. Some artifacts may occur like single pixels with high signal intensity. The loss of signal intensity towards the edges of FOV is caused by the coil geometry used to send and receive the frequency signals. For further details the reader is referred to Mietchen et al. (2005) for fossils and to Ziegler et al. (2011) for living forms.

BGD

10, 18803–18851, 2013

Non-invasive imaging methods in cephalopod research

R. Hoffmann et al.

[Title Page](#)[Abstract](#)[Introduction](#)[Conclusions](#)[References](#)[Tables](#)[Figures](#)[⏪](#)[⏩](#)[◀](#)[▶](#)[Back](#)[Close](#)[Full Screen / Esc](#)[Printer-friendly Version](#)[Interactive Discussion](#)

be produced. This will be post-processed by segmentation, or isosurface rendering. In our example the best result for the rather small *Spirula* shell was obtained from the 60 μm micro-CT scan (Fig. 2f). The constrictions and the protoconch, the first chamber in the center of the shell, are visible in the micro-CT data which is not the case for both surface scans. The polygonal model file size (7.6 MB) is comparable with the 16 μm resolution surface scan, but the size of the raw data is seven times greater. Due to the open and light construction of surface scanners it would be possible to create a polygonal model of the so far largest known ammonite *Parapuzosia seppenradensis* with both sensors (16 μm and 60 μm).

In addition, high resolution surface scanning of objects with a simple geometry (e.g., cubes) contributes to volume calculations in order to achieve an exact buoyancy calculation for chambered cephalopods. We first applied this approach to shells of the extant *Nautilus*, and *Spirula* and transferred it than to the cephalopod group of extinct ammonoids. Therefore we scanned a massive calcite crystal with both sensors (16 μm and 60 μm) of the surface scanner and calculated its volume. With knowledge of its volume (Table 1) obtained from the surface scan the calcite crystal was subsequently scanned together with the cephalopod shells in a micro-CT (see application micro-CT and discussion) acting as a reference body in what is called the quantitative computed tomography (QCT) approach. QCT is a medical technique developed in the 1970s to measure bone density. During this approach a standard material with similar absorption properties (called a phantom) like the material being scanned is used. The object of interest and the phantom are scanned together, in the case of bone the phantom is generally composed of hydroxyapatite (Adams, 2009).

4.2 Computed tomography (CT)

In order to scan objects that exceeded the maximum spatial dimensions for micro- or nano-CT's a medical CT-scanner was used. In addition to the scanning of large specimens, a second application of medical CT-scanners is to perform pre-scans to test rock samples for the content of suitable material (e.g., rare hollow ammonites) and

BGD

10, 18803–18851, 2013

Non-invasive imaging methods in cephalopod research

R. Hoffmann et al.

Title Page

Abstract

Introduction

Conclusions

References

Tables

Figures

◀

▶

◀

▶

Back

Close

Full Screen / Esc

Printer-friendly Version

Interactive Discussion



contemporaneous localization of these fossils within a larger rock sample. Due to their short scan time medical CT-scanners can be used to scan a large amount of material in a short time interval (Fig. 3c). We scanned a completely chambered specimen of the Upper Jurassic lytoceratid ammonite *Lobolytoceras costellatum* from Madagascar with a shell diameter of 61.5 cm and most of its aragonitic shell preserved (Fig. 3a and b). The final part of the conch was filled with calcareous sediment with similar absorption properties compared to the shell which leads to a low SNR hindering a visualization of internal septa (Fig. 3a, white arrow). The inner part of the same specimen was filled with material of different absorption properties compared to the preserved shell allowing the recognition of the complexly folded septa (Fig. 3a, black arrow). Besides the major elements of the septa, the septal lobe – a character that constitutes the monophyly of the Lytoceratoidea (Hoffmann, 2010) is visible in the median plane parallel to the coiling axis (Fig. 3a, red arrows). Growing into an apical direction the internal lobe gets in contact with the preceding septum and is attached on its surface generating the structure called septal lobe. Volume rendering scalar values of the 3-D image is integrated in the direction of the projection producing a transparent image that shows the sedimentary infill of nearly all of the earlier chambers with calcareous mud but also show slight differences between shell and infill imitating a suture line (Fig. 3b). The recognition of internal major structures invisible to the naked eye may be useful for planned subsequent technical preparation of a certain structure (e.g., surface of the ammonoid septum as described for *Lobolytoceras costellatum* by Schreiber and Hoffmann, 2009).

Besides this a first check for the state of preservation can be performed allowing for a decision of further treatment. If the fossil material seems to be suitable the data from the pre-scan can subsequently be used to extract the fossils from the rock by using computer numerical controlled (CNC) devices (saws, mills, water jet cutters). After extracting the fossil from the surrounding rock a high resolution scan is necessary for creating a three dimensional model including all internal and external features of the ammonite. Due to the low resolution of the medical CT surface details and the

BGD

10, 18803–18851, 2013

Non-invasive imaging methods in cephalopod research

R. Hoffmann et al.

Title Page

Abstract

Introduction

Conclusions

References

Tables

Figures



Back

Close

Full Screen / Esc

Printer-friendly Version

Interactive Discussion



thin internal septa of the scanned ammonite are not or hardly visible. Therefore these pre-scans are not suitable to reconstruct fossils with every minute detail.

4.3 Micro-computed tomography (micro-CT)

We scanned a *N. pompilius*, *S. spirula* and a juvenile ammonite (?*Cadoceras* sp.), used as representatives for large, medium and small objects, with the phoenix|x-ray v|tome|x s 240 micro-CT device. The results for the juvenile ?*Cadoceras* will be compared within the synchrotron chapter, and for *Spirula* see the nano-CT chapter.

In this paragraph we focus on one shell of *N. pompilius*, with a diameter of 17 cm, scanned with different resolutions. The obtained data sets were subsequently visualized, segmented and scan artifacts were removed with the software package Avizo Fire 7.0 (Avizo VSG, Düsseldorf, Germany).

In preparation of a final buoyancy calculation a validation test was performed on two datasets of the same *Nautilus* shell, one scanned at a resolution of 172 μm and the second at 190 μm . Both datasets were segmented using the same minimum–maximum threshold values (26 764–64 749). The estimations for the higher resolution scan resulted in a shell weight closer to the true shell weight of 203.5 g (Table 2). The shell volume was multiplied by 2.5 g cm^{-3} and 2.7 g cm^{-3} which were the minimum and maximum density values reported in the literature for aragonitic cephalopod shells (see summary in Hoffmann and Zachow, 2011).

However, the calculated shell weight is far away (up to 23%) from the weighted value which was largely caused by the wrongful manipulation of the threshold but, as will be shown later, also by other sources of error. Therefore we tested the QCT approach with different reference bodies (Al_2O_3 , SiO_2 high precision spheres with a deviation less than 10 μm and a calcite crystal). We scanned the three reference bodies together with the *Nautilus* shell at a resolution of 175 μm (Fig. 5a). For all three reference bodies we determined the threshold for the segmentation tool separately till the selected volume meets the calculated volume of the precision spheres and the calcite crystal. The volume for the calcite crystal was obtained from high resolution (16 μm) surface scans

Title Page

Abstract

Introduction

Conclusions

References

Tables

Figures



Back

Close

Full Screen / Esc

Printer-friendly Version

Interactive Discussion



as mentioned above. The three different threshold values were subsequently applied to segment the shell material.

The smallest deviation from the actual weight and the calculated weight of the *Nautilus* shell was for the SiO₂-sphere and surprisingly the largest for the calcite crystal.

Compared with the values achieved without using a reference body all presented values with the reference bodies are much closer to the actual shell weight (Table 3a). This also hold true after the remaining shell parts (earliest very thin septa) were manually segmented and added to the shell weight (Table 3b). Due to the small volume (less than 0.5 cm³) the weight increase due to the thin shell elements remained small as well. The buoyancy of the fully segmented shell was calculated (Fig. 4).

The large deviation between actual and calculated weight achieved for the calcite crystal may result from the differences in the thickness of both objects (calcite crystal, shell). The differences in the grey scale values seen in the primary image data depend on absorption properties which are related to chemical composition and thickness of the material. Solid material with a high density has lighter grey scale values based on the linear x-ray absorption coefficients compared to thinner material of the same composition, while air remains black. Due to the specific density of the used calcite crystal the grey scale values are comparable to the scanned shells. During ontogeny the shell thickness increases in *Nautilus*, *Spirula* and ammonoids being the thinnest in early ontogenetic stages. In our example latest shell parts including the whole body chamber and the septa of the last whorl of the chambered phragmocone were selected with the threshold determined using the reference bodies. The earliest/thinnest juvenile shell parts are not within the selection due to lower grey scale values. To overcome this problem we manually corrected the threshold to lower values and selected the remaining minor shell parts which may lead to a slight weight increase. Another agent that causes problems in exact determination of volumes in a 3-D data set is the partial volume effect (PVE). The volume of a certain structure varies with different applied thresholds for segmentation. This problem is due to different voxel intensities seen as different grey scales in the resulting image depending on the attenuation effects of

Title Page

Abstract

Introduction

Conclusions

References

Tables

Figures



Back

Close

Full Screen / Esc

Printer-friendly Version

Interactive Discussion



Non-invasive imaging methods in cephalopod research

R. Hoffmann et al.

Title Page

Abstract

Introduction

Conclusions

References

Tables

Figures



Back

Close

Full Screen / Esc

Printer-friendly Version

Interactive Discussion



the scanned material the x-rays are passing through. Attenuation of the x-rays mainly depends on the chemical composition of the material and to a minor degree to its density (Stock, 2006). X-rays passing through 100 % shell material or air result in white or black voxel. However, x-rays may pass through 1–100 % of one or the other material (shell/air/surrounding rock) or compound materials with different attenuation properties resulting in different grey scales. These different grey scales cause the PVE when the material was selected using a certain threshold which results in a deviation from the actual weight of the structure of interest e.g., a *Nautilus* shell (Fig. 5b–g).

In addition, scan artifacts may result in similar grey scales like the shell material which sometimes hinder a correct assignment. Thus, the effect of the PVE to volume calculation increases with lower resolution and higher complexity of object morphology. Such an object of complex morphology is the shell of chambered cephalopods, with the highest complexity seen in ammonoids. While the calculated absolute value of volumes may be far away from the actual value the relative changes in the chamber volumes of the *Nautilus* shell are reliable. Hence, to conduct a reliable volumetric analysis the highest resolution available with at best no scan artifacts is necessary. It is suggested to scan at least one reference body, of which the correct volume is precisely known, together with the object under examination. Here we present changes of chamber volumes during ontogeny (Fig. 6) for *Nautilus*. Note the slight decrease of the volumes of the last two chambers indicating that this specimen achieved mature stage and stops shell growth (septal crowding; Collins and Ward, 2010).

Finally, slight changes in the shell density between conch and septa (Hoffmann and Zachow, 2011) may result in deviations, too. Therefore septa and conch wall should be segmented as individual materials.

Less problematic compared to a volumetric analysis is to measure distances and angles in 3-D data sets. Deviations that may occur are small and limited to 2–6 voxel. In case of the *Nautilus* shell (of 17 cm in diameter scanned with a resolution of 190 μm) the measured diameter, and all other measured distances, vary between 17 cm \pm 0.114 cm which is below 1 % (0.67 %). The model of the *Nautilus* was virtually cut along stan-

BGD

10, 18803–18851, 2013

Non-invasive imaging
methods in
cephalopod research

R. Hoffmann et al.

Title Page

Abstract

Introduction

Conclusions

References

Tables

Figures

⏪

⏩

◀

▶

Back

Close

Full Screen / Esc

Printer-friendly Version

Interactive Discussion



standardized axes (see above). Standardized distances were now measured every 10° . Using physical specimens cross cut measuring is only possible every 180° or at best 90° after a second cross cut perpendicular to the first one. In comparison, with virtual clipping, measurements can be taken at every single degree for a precise description of ontogenetic changes. Therefore with virtual clipping more data for the same morphology or structure become available. According to Korn (2010) the most important ontogenetic trajectories used in the literature to describe coiled cephalopod conchs for *Nautilus* are shown in Figs. 6 and 7. These are the Whorl Width Index (WWI), Umbilical Width Index (UWI), Whorl Expansion Rate (WER), and Conch Width Index (CWI). Besides these parameters additional characters for species description become available; e.g., septal spacing (Fig. 6e), siphuncle thickness and position, length of the juvenile shell (rotation angle to the nepionic constriction), length of the body chamber among others.

We report a marked shift to lower values between septa seven and nine indicating the moment of hatching in *Nautilus* according to Arnold et al. (2010). Between septum 9 and 30 the septal spacing remains more or less stable resulting in a linear increasing total rotational angle. For the last few chambers the septal spacing again shows a marked shift to lower values (Fig. 6e) indicating the adult stage of the animal which is accompanied by the stop of shell growth causing septal crowding and a decreasing chamber volume (Fig. 6d).

Recently, Kerbl et al. (2013) applied micro-CT scanning together with contrast-enhancing substances for 3-D imaging of the soft bodied cephalopod *Euprymna*. Based for 14 specimens these authors reconstructed the ontogenetic development of the nervous system of *Euprymna* showing that ontogeny can also be analyzed from soft tissues using micro-CT technology.

4.4 Nanofocus-computed tomography (nano-CT)

Based on the observations of Brunke et al. (2008) and our own experiences the nano-CT fills the gap between micro-CT and SR μ CT with respect to resolution and contrast

BGD

10, 18803–18851, 2013

Non-invasive imaging
methods in
cephalopod research

R. Hoffmann et al.

Title Page

Abstract

Introduction

Conclusions

References

Tables

Figures



Back

Close

Full Screen / Esc

Printer-friendly Version

Interactive Discussion



properties of the produced images. Compared to a synchrotron facility setup the access to a nano-CT is much easier. We ran several tests with the shell of *Spirula spirula* and the shell of a juvenile ?*Cadoceras*. Due to the high resolution scans the PVE will be negligible and is not discussed. Here we describe minute structures of the shell of *Spirula* that become visible while the nano-CT data for the juvenile ?*Cadoceras* will be compared with SR μ CT- and micro-CT derived images in the following chapter. Due to the high resolution (8.7 μ m) 2-D measurements are highly precise and since the PVE is minor the same holds true for volumes. Quantification of morphological characters and volumes as well as ontogenetic changes back to the very first chamber (protoconch) with its 1–2 μ m thick shell wall including buoyancy calculation becomes available with necessary precision.

In contrast to surface scanning or 60 μ m resolution micro-CT scans the high resolution scans of the nano-CT enable the recognition of very minute conch features like the pillar zone of the siphuncle, attachment scars on the inner surface of every chamber, and minute crenulation of the shell surface resulting from the attachment of the soft body along the outer surface of the shell (Fig. 8c). Reticulate pattern disappear at the ventral area and along the margin of the aperture (Fig. 8a) where the soft body obviously was not attached to the shell.

Applied to the extinct ammonoids exact morphological data becomes available for the description of features of the ammonitella, the ammonite hatchling shell, or muscle attachment sites of the soft body to the shell wall (Doguzhaeva and Mutvei, 1996; Shigeta, 1993). Morphology of the ammonitella was used to distinguish between major ammonoid groups based on protoconch size and shape, fixator length and position, position of the siphuncle, length/angle of the ammonitella and the nepionic constriction. Internal structures like septal- and conch wall thickness, siphuncle thickness of the ammonitella were achieved by cross sections. External shell features like crenulation as shown for *Spirula* (Fig. 9), which are also present on juvenile gastropod shells (Bandel, 1982), can be traced and used for the discussion if ammonoids had an internal or external shell (Doguzhaeva and Mutvei, 1996). However, the high scan-resolution makes

the nano-CT a useful tool for microfossils like Foraminifera or Ostracoda with complex internal shell structures (Briguglio et al., 2011; Görög et al., 2012; Hohenegger and Briguglio, 2012).

4.5 Synchrotron radiation based micro-computed tomography (SR μ CT)

5 The SR μ CT technology using monochromatic x-ray beams produced with very high intensity resulting in accurate absorption information and achieves the highest contrasts and highest resolutions available today. Compared to the reconstructed data of a polychromatic μ CT scan the images of a monochromatic SR μ CT scan seem precise and sharp and not blurred with scan artifacts like bright rings (Fig. 10). Due to the
10 very high resolution (down to 0.7 μ m at the ESRF; Tafforeau and Smith, 2013) and the precision of SR μ CT scans this technique is of increasing interest for very small specimens and delicate structures (Prymak et al. (2005) quantified the shell thickness of a 120 h old gastropod shell) even if preserved within surrounding rocks. Recently, Kruta et al. (2011) were able to present a reconstruction of a full buccal apparatus, including the radula, of a Mesozoic ammonite (*Baculites*, Upper Cretaceous) using SR μ CT
15 technology, where most of the single radula tooth elements had a size of 500 μ m. In order to compare the results of a SR μ CT scan with other CT techniques we used three different juvenile ammonites of ?*Cadoceras* sp. All specimens are coming from the same locality and have the original aragonitic shell preserved. The reconstructed
20 images of the micro-CT with a low SNR results in relatively poor contrast in the grey scale images. The septa of the first specimen appear thicker than expected for this ontogenetic stage (Fig. 10a) and led to the unproved assumption that some other material with similar absorption properties has covered the primary shell material. The images from the nano-CT, with a sharper contrast, reveal secondary calcite crystals with pronounced growth in apertural direction (Fig. 10b) in the second specimen. Due
25 to the precision of the high resolution scan even the nepionic constriction (Fig. 10b and c; green arrow) which indicates the moment of hatching in ammonoids is visible. The sharpest result with highest contrast was achieved using SR μ CT. The images show

Title Page

Abstract

Introduction

Conclusions

References

Tables

Figures



Back

Close

Full Screen / Esc

Printer-friendly Version

Interactive Discussion



Non-invasive imaging methods in cephalopod research

R. Hoffmann et al.

Title Page

Abstract

Introduction

Conclusions

References

Tables

Figures

◀

▶

◀

▶

Back

Close

Full Screen / Esc

Printer-friendly Version

Interactive Discussion



a secondary layer of calcite crystals on the inner shell surface of the third specimen. The amount of crystal growth differs between the three different specimens used in our study. The documented crystal growth has to be taken into account during the subsequent segmentation process where it should be avoided to include crystals in the shell material otherwise a buoyancy calculation will fail. Our observation of secondary calcite crystals within the chambers of hollow ammonites with their original shell (aragonitic nacre) preserved is interesting for geochemists too. The crystals are up to ten times thicker than the original shell material and contain different isotope and trace element signatures compared to the ammonoid nacre (Fig. 10f, white arrow). Since the standard procedure for isotopic analysis contains the process of sample powdering this means a mixed signal will be obtained not representing the sole isotope signal of the ammonoids ambient seawater during lifetime. Due to the assumed early diagenetic growth of secondary calcite crystals within the ammonoids shell these will record a bottom water signal that will hamper a correct paleo-seawater temperature reconstruction (see also Marshall, 1981). A sufficient resolution and SNR to distinguish between primary shell and secondary calcite was only possible with SR μ CT technology.

4.6 Magnetic Resonance Imaging (MRI)

MRI has been rarely applied to extant (*Sepia* in Quast et al., 2001, and in Ziegler et al., 2011; *Lolliguncula* in Gozansky et al., 2003; *Loligo* in Mooney et al., 2010) or fossil cephalopod material (belemnites in Mietchen et al., 2005). In case of belemnites (ten armed coleoids) this technique elucidated paleopathological and paleoecological questions (Fig. 11). Measurements were made with a BRUKER[®] Advance NMR spectrometer operating at a ¹H resonance frequency of 400 MHz with standard Micro2.5 microimaging equipment and a maximum gradient strength of 0.4 T m⁻¹. The images of the pathological belemnite rostra were recorded using a 3-D spin-echo imaging sequence (Mietchen et al., 2005). With the sample dimensions of about 10 mm × 10 mm × 30 mm a resolution of 100 μ m was obtained. The total data acquisition time depends on the sample's signal strength but was in our case not less than 18 h. In fossil material hydro-

Non-invasive imaging methods in cephalopod research

R. Hoffmann et al.

Title Page

Abstract

Introduction

Conclusions

References

Tables

Figures

◀

▶

◀

▶

Back

Close

Full Screen / Esc

Printer-friendly Version

Interactive Discussion



gen nuclei (protons) can be used as agents for MRI. Since water is the contrast agent for MRI this non-invasive technique may become an important tool for 3-D reconstructions of dissolved aragonite shells within rocks. The space between internal mould and surrounding rocks can be flooded with water using a vacuum for one or two weeks. MRI provides a better edge resolution and finer details compared to CT scans of comparable resolution. These properties can be improved by using contrast agents such as gadodiamide solution or other substances with paramagnetic properties that decrease or increase the local MRI signal (Clark et al., 2004; Ziegler et al., 2011). This may be of special interest for species with a highly complex morphology, which are normally hard to mold with putty, like the heteromorph ammonite *Nipponites*. Problems may occur if liquid penetration into unconnected voids is limited by the porosity and permeability of the encapsulating sediment. Bubbles cause artifacts on the images and have to be extracted from the structure of interest before scanning takes place or needs to be removed virtually during the post-processing step.

5 Summary

Our investigations demonstrate that non-invasive imaging methods are a powerful tool to sharpen the species concept by achieving more data for certain morphologies compared to the standard procedure (cutting specimens) and therefore should be applied whenever possible. It also shows that exact buoyancy calculation of Recent and extinct cephalopods are approachable by applying the methods described above.

The species concept in paleontology is purely based on morphology. Non-invasive imaging methods can contribute to this concept also by making additional internal morphological structures (e.g., septal spacing) available by keeping the fossil undamaged. Our presented applications show with a reasonable amount of specimens at hand non-invasive methods are suitable to improve taxonomic schemes and our understanding of phylogenetic relationships between higher ammonoid taxa and the intraspecific variability of ammonoids. For example the ammonoid taxon *Svalbardiceras* shows a high

morphological plasticity (Weitschat, 2008) while other taxa show only very small variations in their shell morphology like most of the lytoceratids (Hoffmann, 2010). The use of CT images and 3-D models improves the description of the internal and external morphology of cephalopod shells.

By using non-invasive methods more data points become available for the same morphology/structure and therefore improve the morphological species concept. The application of high resolution CT scans reveals internal morphological features like septal spacing, -thickness, and -shape, conch wall thickness, position and diameter of the siphuncle, and from the ammonitella the dimension of the protoconch, caecum, ammonitella angle, length of the fixator among others.

An important character complex is the suture line. The suture line is the result of the connection of the septa with the inner surface of the conch wall. Juvenile and adult suture lines have been used to distinguish between major ammonoid taxa (Schindewolf, 1961–1968). Using non-invasive methods the ontogenetic development of the suture line is easier to observe. Due to their accretionary growth cephalopods are ideal candidates to study ontogenetic changes of their morphology in extant species (*Nautilus*, *Spirula*) and evolutionary ontogenetic shifts through time in ammonoids. Another important feature is the connection site of the soft body to the shell – the so called attachment scars. As far as we know no study about ontogenetic changes of attachment scars is available for cephalopods (Fig. 9b). Significant changes of these scars can be compared with changes in morphology and if they occur contemporaneous or not. This knowledge is crucial for functional morphology and/or paleobiological reconstructions. All of these characters are important morphological features that will improve the data base used for future cladistic analysis.

Besides new 2-D morphological information our results show that the application of non-invasive methods will improve our understanding of cephalopod functional morphology by exact determination of 3-D values. Important prerequisites in order to perform a most exact determination of volumes and areas (chamber, shell and septum) are: highest possible resolution, good SNR, reconstruction algorithms that distinguish

BGD

10, 18803–18851, 2013

Non-invasive imaging methods in cephalopod research

R. Hoffmann et al.

Title Page

Abstract

Introduction

Conclusions

References

Tables

Figures



Back

Close

Full Screen / Esc

Printer-friendly Version

Interactive Discussion



Non-invasive imaging methods in cephalopod research

R. Hoffmann et al.

Title Page

Abstract

Introduction

Conclusions

References

Tables

Figures

◀

▶

◀

▶

Back

Close

Full Screen / Esc

Printer-friendly Version

Interactive Discussion

and paleobiology of ammonoids (Westermann, 1993). Furthermore, there exists a century old debate concerning the main function of the complexly fluted ammonite septa (summarized in Hoffmann, 2010). Hitherto, the function mainly was discussed on the basis of mathematical models and two major interpretations arose. One postulates a mechanical strengthening of the shell against hydrostatic pressure, while the other favors physiological reasons (pumping out and refill of chamber liquid). During the last two decades two attempts were made to solve this problem with the help of mathematical algorithms and computers (Daniel et al., 1997; Hassan et al., 2002) resulting in opposite results. Our applications show a potential in 3-D models obtained from original fossil material to greatly contribute to this discussion.

Acknowledgements. The authors are grateful to G. Fritsch (Kleintierklinik, Düppel, Berlin, Germany), J. Goebbels working group (Bundesanstalt für Materialforschung und -prüfung, Berlin, Germany), L. Heuser and W. Weber (Universitätsklinikum Knappschafts-Krankenhaus Bochum) for several CT scannings, D. Mietchen (Fraunhofer-Institute, St. Ingberg and Saarbrücken, Germany) for Biomedical Engineering (IBMT), S. Ingbert (Faculty of Physics and Mechatronics, University of the Saarland, Saarbrücken, Germany) for MRI imaging. A. Ziegler provided information about MRI imaging. M. Ehlke (Zuse Institut Berlin) for helping us with several problems concerning the CT-data analyses. V. Mitta (Moscow) and J. Gründel (Freie Universität Berlin, Germany) donated small juvenile ammonoids and Y. Shigeta (National Museum of Nature and Science, Department of Geology and Paleontology, Division of Paleoenvironment and Paleocology, Tokyo, Japan) for the loan of the hollow specimen of *Gaudryceras* presented in this study. RH acknowledges the financial support of DFG (Project-No.: HO 4674/2-1).

References

- Adams, J. E.: Quantitative computed tomography, *Eur. J. Radiol.*, 71, 415–424, doi:10.1016/j.ejrad.2009.04.074, 2009.
- Anderson, P. S. L., Bright, J. A., Gill, P. G., Palmer, C., and Rayfield, E. J.: Models in palaeontological functional analysis, *Biol. Letters*, 8, 119–122, doi:10.1098/rsbl.2011.0674, 2012.
- Arnold, J. M., Landman, N. H., and Mutvei, H.: Development of the embryonic shell of *Nautilus*, in: *Nautilus – The Biology and Paleobiology of a Living Fossil*, reprint with additions, edited

by: Saunders, W. B. and Landman, N. H., Topics in Geobiology, Springer Netherlands, 373–400, 2010.

Bandel, K.: Morphologie und Bildung der frühontogenetischen Gehäuse bei conchiferen Mollusken, *Facies*, 7, 1–198, doi:10.1007/bf02537225, 1982.

5 Bonse, U. and Busch, F.: X-ray computed microtomography (μ CT) using synchrotron radiation (SR), *Prog. Biophys. Mol. Bio.*, 65, 133–169, 1996.

Briguglio, A., Metscher, B., and Hohenegger, J.: Growth rate biometric quantification by x-ray microtomography on larger benthic Foraminifera: three-dimensional measurements push nummulitids into the fourth dimension, *Turk. J. Earth Sci.*, 20, 683–699, doi:10.3906/yer-0910-44, 2011.

10 Brunke, O., Brockdorf, K., Drews, S., Müller, B., Donath, T., Herzen, J., and Beckmann, F.: Comparison between x-ray tube-based and synchrotron radiation-based μ CT, *Proc. SPIE 7078, Developments in X-Ray Tomography VI*, 70780U, San Diego, California, USA, 10 August, 1–12, doi:10.1117/12.794789, 2008.

15 Callaghan, P. T.: Principles of Nuclear Magnetic Resonance Microscopy, Oxford University Press, Clarendon, 1991.

Clark, N. D. L., Adams, C., Lawton, T., Cruickshank, A. R. I., and Woods, K.: The Elgin marvel: using magnetic resonance imaging to look at a mouldic fossil from the Permian of Elgin, Scotland, UK, *Magn. Reson. Imaging*, 22, 269–273, doi:10.1016/j.mri.2003.09.006, 2004.

20 Collins, D. and Ward, P. D.: Adolescent growth and maturity in *Nautilus*, in: *Nautilus – The Biology and Paleobiology of a Living Fossil*, reprint with additions, edited by: Saunders, W. B. and Landman, N. H., Topics in Geobiology, Springer Netherlands, 421–432, 2010.

Daniel, T. L., Helmuth, B. S., Saunders, W. B., and Ward, P. D.: Septal complexity in ammonoid cephalopods increased mechanical risk and limited depth, *Paleobiology*, 23, 470–481, doi:10.1666/0094-8373-23.4.470, 1997.

25 Davis, G. R. and Elliott, J. C.: Artefacts in X-ray microtomography of materials, *Mater. Sci. Tech. Ser.*, 22, 1011–1018, doi:10.1179/174328406x114117, 2006.

Doguzhaeva, L. A. and Mutvei, H.: Attachment of the body to the shell in ammonoids, in: *Ammonoid Paleobiology*, edited by: Landman, N. H., Tanabe, K., and Davis, R. A., Topics in Geobiology, 13, Plenum Press, New York, 43–63, 1996.

30 Drews, S., Beckmann, F., Herzen, J., Brunke, O., Salmon, P., Friess, S., Laib, A., Koller, B., Hemberger, T., Müller-Gerbl, M., and Müller, B.: Comparative micro computed tomography

BGD

10, 18803–18851, 2013

Non-invasive imaging methods in cephalopod research

R. Hoffmann et al.

Title Page

Abstract

Introduction

Conclusions

References

Tables

Figures

◀

▶

◀

▶

Back

Close

Full Screen / Esc

Printer-friendly Version

Interactive Discussion



Non-invasive imaging methods in cephalopod research

R. Hoffmann et al.

Title Page

Abstract

Introduction

Conclusions

References

Tables

Figures

◀

▶

◀

▶

Back

Close

Full Screen / Esc

Printer-friendly Version

Interactive Discussion



study of a vertebral body, Proc. SPIE 7078, Developments in X-Ray Tomography VI, 70780C, 1–14, doi:10.1117/12.793815, 2008.

Falkingham, P. L.: Acquisition of high resolution 3-D models using free, open-source, photogrammetric software, Palaeontol. Electron., 15, 1T:15p, 2012.

5 Görög, Á., Szinger, B., Tóth, E., and Viszok, J.: Methodology of the micro-computer tomography on Foraminifera, Palaeontol. Electron., 15, 3T:15p, 2012.

Gozansky, E. K., Ezell, E. L., Budelmann, B. U., and Quast, M. J.: Magnetic resonance histology: in situ single cell imaging of receptor cells in an invertebrate (*Lolliguncula brevis*, Cephalopoda) sense organ, Magn. Reson. Imaging, 21, 1019–1022, doi:10.1016/S0730-725X(03)00215-7, 2003.

10 Gray, F.: Pulse code communication, 17 March 1953, United States Patent no. 2,632,058, 1953.

Hassan, M. A., Westermann, G. E. G., Hewitt, R. A., and Dokainish, M. A.: Finite-element analysis of simulated ammonoid septa (extinct Cephalopoda): septal and sutural complexities do not reduce strength, Paleobiology, 28, 113–126, doi:10.1666/0094-8373(2002)028<0113:feaosa>2.0.co;2, 2002.

15 Herbert, M. H., Jones, C. B., and Tudhope, D. S.: Three-dimensional reconstruction of geoscientific objects from serial sections, Visual Comput., 11, 343–359, doi:10.1007/bf01909875, 1995.

Hoffmann, R.: New insights on the phylogeny of the Lytoceratoidea (Ammonitina) from the septal lobe and its functional interpretation, Rev. Paleobiol., 29, 1–156, 2010.

Hoffmann, R., and Zachow, S.: Non-invasive approach to shed new light on the buoyancy business of chambered cephalopods (Mollusca), in: Mathematical geosciences at the crossroads of theory and practice, edited by: Marschallinger, R. and Zobl, F., Proceedings IAMG 2011 conference, Salzburg, 506–516, doi:10.5242/iamg.2011.0163, 2011.

25 Hoffmann, R., Zachow, S., Füsseis, F., and Korn, D.: Quantitative morphology using x-ray computed tomography and the species concept in palaeontology: a case study from cephalopods, Terra Nostra, 2012, 80–81, 2012.

Hohenegger, J. and Briguglio, A.: Axially oriented sections of nummulitids: a tool to interpret larger benthic foraminiferal deposits, J. Foramin. Res., 42, 134–142, doi:10.2113/gsjfr.42.2.134, 2012.

30 Hurum, J. H.: Three-dimensional reconstruction in palaeontology, GFF, 118, 60, doi:10.1080/11035899609546345, 1996.

Non-invasive imaging methods in cephalopod research

R. Hoffmann et al.

Title Page

Abstract

Introduction

Conclusions

References

Tables

Figures

◀

▶

◀

▶

Back

Close

Full Screen / Esc

Printer-friendly Version

Interactive Discussion



Kerbl, A., Handschuh, S., Nödl, M.-T., Metscher, B., Walzl, M., and Wanninger, A.: Micro-CT in cephalopod research: investigating the internal anatomy of a sepiolid squid using a non-destructive technique with special focus on the ganglionic system, *J. Exp. Mar. Biol. Ecol.*, 447, 140–148, doi:10.1016/j.jembe.2013.02.022, 2013.

5 Korn, D.: A key for the description of Palaeozoic ammonoids, *Foss. Rec.*, 13, 5–12, doi:10.1002/mmng.200900008, 2010.

Korn, D.: Quantification of ontogenetic allometry in ammonoids, *Evol. Dev.*, 14, 501–514, doi:10.1111/ede.12003, 2012.

10 Kruta, I., Landman, N., Rouget, I., Cecca, F., and Tafforeau, P.: The role of ammonites in the Mesozoic marine food web revealed by jaw preservation, *Science*, 331, 70–72, doi:10.1126/science.1198793, 2011.

Lehmann, W. M.: Stereo-röntgenaufnahmen als hilfsmittel bei der untersuchung von versteinierungen, *Natur und Museum*, 62, 323–330, 1932.

15 Luo, Z. and Ketten, D. R.: CT scanning and computerized reconstructions of the inner ear of multituberculate mammals, *J. Vertebr. Paleontol.*, 11, 220–228, doi:10.1080/02724634.1991.10011389, 1991.

Marks II, R. J.: Introduction to Shannon Sampling and Interpolation Theory, Springer-Verlag, New York, 324 pp., 1991.

20 Marshall, J. D.: Zoned calcites in Jurassic ammonite chambers: trace elements, isotopes and neomorphic origin, *Sedimentology*, 28, 867–887, doi:10.1111/j.1365-3091.1981.tb01949.x, 1981.

Mietchen, D., Keupp, H., Manz, B., and Volke, F.: Non-invasive diagnostics in fossils – Magnetic Resonance Imaging of pathological belemnites, *Biogeosciences*, 2, 133–140, doi:10.5194/bg-2-133-2005, 2005.

25 Mooney, T. A., Hanlon, R. T., Christensen-Dalsgaard, J., Madsen, P. T., Ketten, D. R., and Nachtigall, P. E.: Sound detection by the longfin squid (*Loligo pealeii*) studied with auditory evoked potentials: sensitivity to low-frequency particle motion and not pressure, *J. Exp. Biol.*, 213, 3748–3759, doi:10.1242/jeb.048348, 2010.

30 Naglik, C., Monnet, C., Götz, S., Kolb, C., De Baets, K., Tajika, A., and Klug, C.: Growth trajectories of some major ammonoid subclades using grinding tomography data, *Lethaia*, submitted, 2013.

Non-invasive imaging methods in cephalopod research

R. Hoffmann et al.

Title Page

Abstract

Introduction

Conclusions

References

Tables

Figures

◀

▶

◀

▶

Back

Close

Full Screen / Esc

Printer-friendly Version

Interactive Discussion

Pascual-Cebrian, E., Hennhöfer, D., and Götz, S.: 3-D morphometry of polyconitid rudist bivalves based on grinding tomography, *Facies*, 59, 347–358, doi:10.1007/s10347-012-0310-8, 2013.

5 Prymak, O., Tiemann, H., Sötje, I., Marxen, J., Klocke, A., Kahl-Nieke, B., Beckmann, F., Donath, T., and Epple, M.: Application of synchrotron-radiation-based computer microtomography (SRIC) to selected biominerals: embryonic snails, statoliths of medusae, and human teeth, *J. Biol. Inorg. Chem.*, 10, 688–695, doi:10.1007/s00775-005-0023-3, 2005.

10 Quast, M. J., Neumeister, H., Ezell, E. L., and Budelmann, B. U.: MR microscopy of cobalt-labeled nerve cells and pathways in an invertebrate brain (*Sepia officinalis*, Cephalopoda), *Magn. Reson. Med.*, 45, 575–579, doi:10.1002/mrm.1078, 2001.

Rahman, I. A., Adcock, K., and Garwood, R. J.: Virtual fossils: a new resource for science communication in paleontology, *Evo. Edu. Outreach*, 5, 635–641, doi:10.1007/s12052-012-0458-2, 2012.

15 Schindewolf, O. H.: Studien zur Stammesgeschichte der Ammoniten, *Abh. Akad. Wiss. Lit. Mainz, Math.-Naturw. Kl.*, 1960–1968, 1–901, 1961–1968.

Schreiber, G. and Hoffmann, R.: Der Septallobus als diagnostisches Merkmal für die Überfamilie *Lycoceratoidea* (Cephalopoda: Ammonitina), *Berliner Paläobiologische Abhandlungen*, 10, 307–310, 2009.

20 Shigeta, Y.: Post-hatching early life history of Cretaceous Ammonoidea, *Lethaia*, 26, 133–145, doi:10.1111/j.1502-3931.1993.tb01804.x, 1993.

Sollas, I. B. J. and Sollas, W. J.: A study of the skull of a *Dicynodon* by means of serial sections, *Philos. T. R. Soc. B*, 204, 201–225, 1914.

Sollas, W. J.: A method for the investigation of fossils by serial sections, *Philos. T. R. Soc. B*, 196, 259–265, 1904.

25 Stock, S. R.: *Microcomputed Tomography – Methodology and Applications*, CRC Press, Taylor and Francis Group, Boca Raton, 331 pp., 2006.

Sutton, M. D., Briggs, D. E. G., Siveter, D. J., and Siveter, D. J.: Methodologies for the visualization and reconstruction of three-dimensional fossils from the Silurian Herefordshire Lagerstätte, *Palaeontol. Electron.*, 4, art.1:17p., 2001.

30 Tafforeau, P. and Smith, T.: Synchrotron virtual palaeohistology: accessing the archives of hominin dental development and life history non-destructively, 11th International Conference on Tooth Morphogenesis and Differentiation, 21, 2013.

Non-invasive imaging methods in cephalopod research

R. Hoffmann et al.

Title Page

Abstract

Introduction

Conclusions

References

Tables

Figures

◀

▶

◀

▶

Back

Close

Full Screen / Esc

Printer-friendly Version

Interactive Discussion



- Tafforeau, P., Boistel, R., Boller, E., Bravin, A., Brunet, M., Chaimanee, Y., Cloetens, P., Feist, M., Hozzowska, J., Jaeger, J.-J., Kay, R. F., Lazzari, V., Marivaux, L., Nel, A., Nemoz, C., Thibault, X., Vignaud, P., and Zabler, S.: Applications of X-ray synchrotron microtomography for non-destructive 3-D studies of paleontological specimens, *Appl. Phys. A-Mater.*, 83, 195–202, doi:10.1007/s00339-006-3507-2, 2006.
- 5 Tipper, J. C.: The study of geological objects in three dimensions by the computerized reconstruction of serial sections, *J. Geol.*, 84, 476–484, 1976.
- Warnke, K. M. and Boletzky, S. V.: The “ventral rib” of the shell in *Spirula* (Cephalopoda, Coleoidea): a cryptic rostrum?, *Berliner Paläobiologische Abhandlungen*, 10, 357–359, 10
2009.
- Weitschat, W.: Intraspecific variation of *Svalbardiceras spitzbergensis* (Frebald) from the Early Triassic (Spathian) of Spitsbergen, *Polar Res.*, 27, 292–297, doi:10.1111/j.1751-8369.2008.00041.x, 2008.
- Westermann, G. E. G.: On alleged negative buoyancy of ammonoids, *Lethaia*, 26, 246, 15
doi:10.1111/j.1502-3931.1993.tb01526.x, 1993.
- Withers, P. J.: X-ray nanotomography, *Mater. Today*, 10, 26–34, doi:10.1016/S1369-7021(07)70305-X, 2007.
- Ziegler, A., Kunth, M., Mueller, S., Bock, C., Pohmann, R., Schröder, L., Faber, C., and Giritbet, G.: Application of magnetic resonance imaging in zoology, *Zoomorphology*, 130, 227–20
254, doi:10.1007/s00435-011-0138-8, 2011.

BGD

10, 18803–18851, 2013

Non-invasive imaging methods in cephalopod research

R. Hoffmann et al.

Title Page

Abstract

Introduction

Conclusions

References

Tables

Figures

◀

▶

◀

▶

Back

Close

Full Screen / Esc

Printer-friendly Version

Interactive Discussion



Table 1. Calculated densities of a calcite crystal (29.2 g) using the polygonal models made from surface and micro-CT scans at different resolutions. The volumes of the polygonal models were measured using PolyWorks/IMEdit®.

scan (resolution)	volume [mm ³]	density [gcm ⁻³]
surface scan (60 μm)	10 958.7	2.665
surface scan (16 μm)	10 900.5	2.679
micro-CT scan (60 μm)	10 925.6	2.673

Non-invasive imaging methods in cephalopod research

R. Hoffmann et al.

Title Page

Abstract

Introduction

Conclusions

References

Tables

Figures



Back

Close

Full Screen / Esc

Printer-friendly Version

Interactive Discussion



Table 2. Influence of the scan resolution to volume/weight calculations of the *Nautilus* shell (actual weight 203.5 g), with minor corrections for artifacts. Only shell material that was selected with the obtained threshold is considered here, no attempt to manually segment unselected shell material (thin septa).

Resolution [μm]	volume [mm ³]	Shell weight [g] with 2.5 g cm ⁻³ 2.7 g cm ⁻³	difference from the actual weight [%]
190	94 679.95	236.70	+15.08
		255.63	+22.71
172	90 179.10	225.45	+10.23
		243.48	+17.89

Non-invasive imaging methods in cephalopod research

R. Hoffmann et al.

Table 3. Influence of different reference bodies at the same resolution (175 μm) to volume/weight calculations of the *Nautilus* shell (203.5 g) with: (A) minor corrections for artifacts, only shell material that was selected with the obtained threshold is considered here, no attempt to manually segment unselected shell material (thin septa), and (B) fully segmented and corrected models.

reference body	A <i>Nautilus</i> shell			B <i>Nautilus</i> shell				
	volume [mm ³]	density [g cm ⁻³]	volume [cm ³]	weight [g] with 2.5 g cm ⁻³ 2.7 g cm ⁻¹	difference from actual weight [%]	volume [cm ³]	weight [g] with 2.5 g cm ⁻³ 2.7 g cm ⁻¹	difference from actual weight [%]
Al ₂ O ₃ -sphere (Ø 22 mm)	5575.28	3.75–3.9	76.52	191.30 206.60	-6.18 +1.51	76.83	192.06 207.43	-5.80 +1.91
SiO ₂ -sphere (Ø 20 mm)	4188.8	2.5	80.01	200.02 216.03	-1.73 +6.00	80.18	200.46 216.50	-1.51 +6.19
calcite crystal (29.2 g)	10 900.5	2.68	84.02	210.05 226.85	+3.19 +10.87	85.49	213.73 230.83	+4.90 +12.58

Title Page

Abstract

Introduction

Conclusions

References

Tables

Figures



Back

Close

Full Screen / Esc

Printer-friendly Version

Interactive Discussion



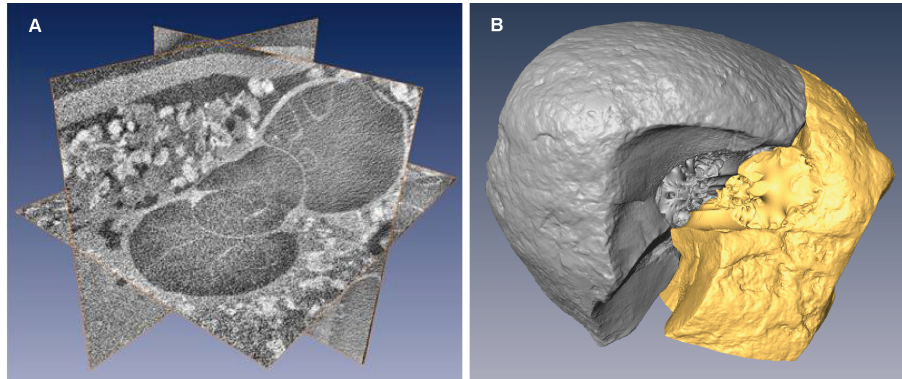


Fig. 1. Multiplanar reconstructions (MPR). **(A)** Tomographic dataset of a hollow Lower Jurassic (Toarcian) *Eleganticeras* (about 1 cm in diameter) with a size of 9 GB, acquired with a v|tome|x s (180 kV tube current, res. 6 μ m). MPR and visualization obtained with the 3-D software ZIBAmira. **(B)** Digitally merged dataset of two separately scanned (res. 45 μ m) parts of a broken Upper Cretaceous concretion of about 13 cm in diameter that contains one specimen of *Gaudryceras* sp. (about 8 cm in diameter, coll. Y. Shigeta, Tokyo).

**Non-invasive imaging
methods in
cephalopod research**

R. Hoffmann et al.

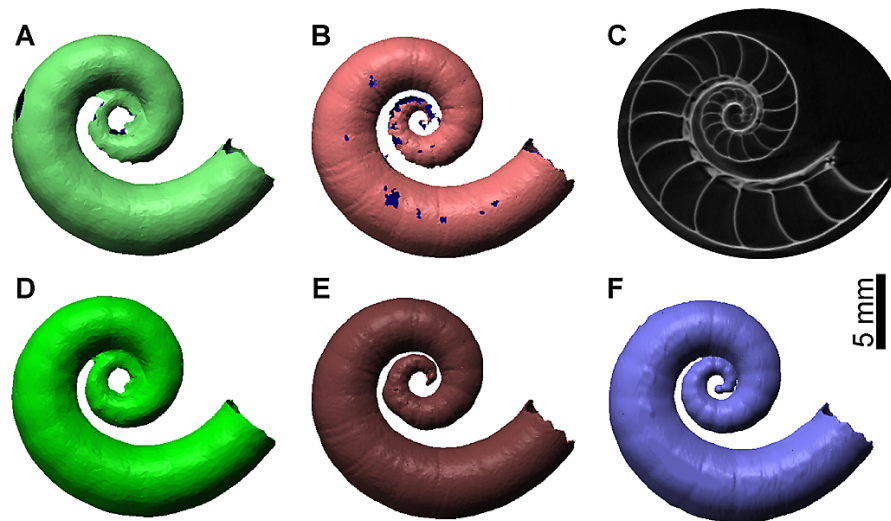


Fig. 2. Raw scans (A–C) and post-processed polygonal models (D–F) of *Spirula spirula* (1.6 cm in diameter). (A and D) surface scan with 60 μm resolution; (B and E) surface scan with 16 μm resolution; (C and F) micro-CT scan with 60 μm resolution; while (C) is a single slice of the micro CT-scan image stack.

[Title Page](#)[Abstract](#)[Introduction](#)[Conclusions](#)[References](#)[Tables](#)[Figures](#)[◀](#)[▶](#)[◀](#)[▶](#)[Back](#)[Close](#)[Full Screen / Esc](#)[Printer-friendly Version](#)[Interactive Discussion](#)

Non-invasive imaging methods in cephalopod research

R. Hoffmann et al.

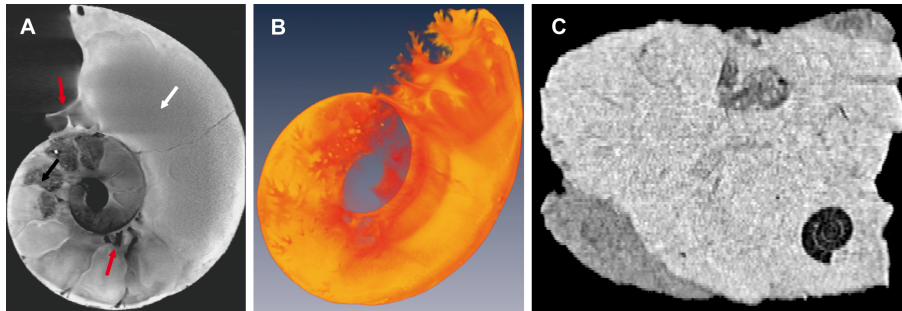


Fig. 3. Medical CT scans of *Lobolytoceras costellatum* (**A** and **B**; scan resolution = 1 mm) from the Oxfordian (Upper Jurassic) of Madagascar (about 61.5 cm in diameter) and *Craspedites* sp. from the Volgian Kostroma region (Russia) (**C**, res. 0.5 mm). (**A**) The specimen lacks the body chamber. The septal lobe (red arrows) is a diagnostic feature of all *Lytoceroidea*. Due to similar density and absorption properties the sediment has a similar grey value compared to the aragonitic shell. Distinguishing between both materials is problematic (white arrow). Different absorption properties of the aragonitic shell and the secondary infill led to better SNR, which allows the recognition of internal structures (black arrow). (**B**) Scalar values of the 3-D image are integrated in the volume rendering in the direction of the projection producing a transparent image, which shows the sedimentary infill. Note the sculptured surface of the last preserved septum. (**C**) Orthoslice of a sediment block (9 cm × 7 cm × 6 cm) pre-scanned in search for hollow material, note one hollow specimen of *Craspedites* sp. in the lower right corner.

Title Page

Abstract

Introduction

Conclusions

References

Tables

Figures

◀

▶

◀

▶

Back

Close

Full Screen / Esc

Printer-friendly Version

Interactive Discussion



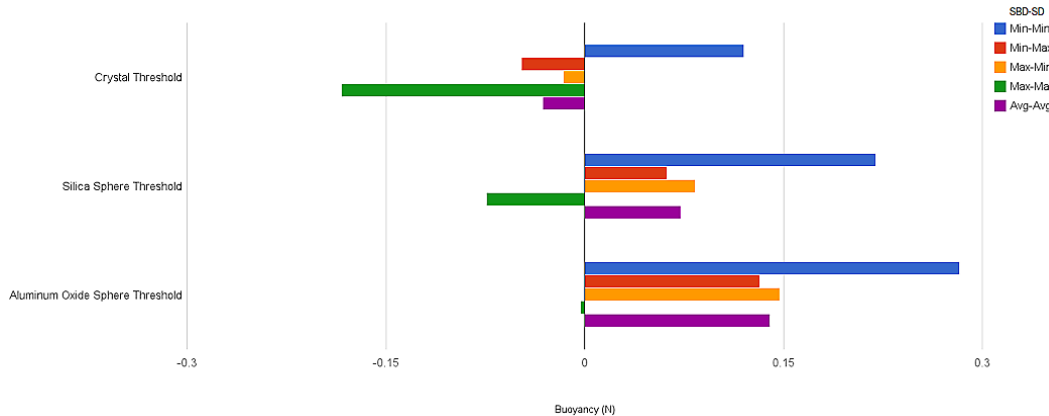


Fig. 4. Buoyancy calculation based on a micro-CT scan (res. 175 μm) of a *Nautilus pompilius* shell together with three reference bodies (phantoms). Used were two high precision spheres (Al_2O_3 , SiO_2) and one calcite crystal. All with exact known dimensions and volumes. For each reference body we present five buoyancy values for different density values for soft body (SBD) and shell (SD) from (Hoffmann and Zachow, 2011). The best approximation is the average-average value. Contrary to the small volume of the shell the different density values have a higher impact on the buoyancy calculation compared to the soft body density which is close to sea water. Buoyancy calculation was operated under the assumption that all phragmocone chambers were gas filled and dry while the body chamber was completely filled with soft tissue.

Title Page

Abstract Introduction

Conclusions References

Tables Figures

◀ ▶

◀ ▶

Back Close

Full Screen / Esc

Printer-friendly Version

Interactive Discussion



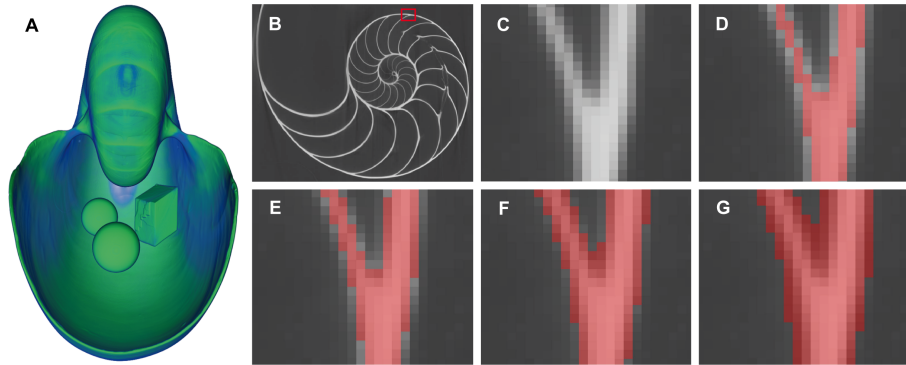


Fig. 5. Partial volume effect (PVE) exemplified for the *Nautilus pompilius* shell (micro-CT scan, res. 175 μm). **(A)** image of the *Nautilus* shell scanned together with three reference bodies (phantoms); **(B)** orthoslice of the same shell; **(C)** close up of **(B)** (red box) showing different grey scales; **(D)** selected shell material after adding a certain threshold value, which may underestimate the true shell volume; **(E)** one voxel was added to the selection shown in **(D)**; **(F)** one voxel was added to the selection shown in **(E)**; **(G)** one voxel was added to the selection shown in **(F)**, which may overestimate the true shell volume. The example demonstrates the importance of a correct threshold value for the material selection to produce a polygonal model with the highest approximation to the original shell.

Title Page

Abstract

Introduction

Conclusions

References

Tables

Figures

⏪

⏩

◀

▶

Back

Close

Full Screen / Esc

Printer-friendly Version

Interactive Discussion



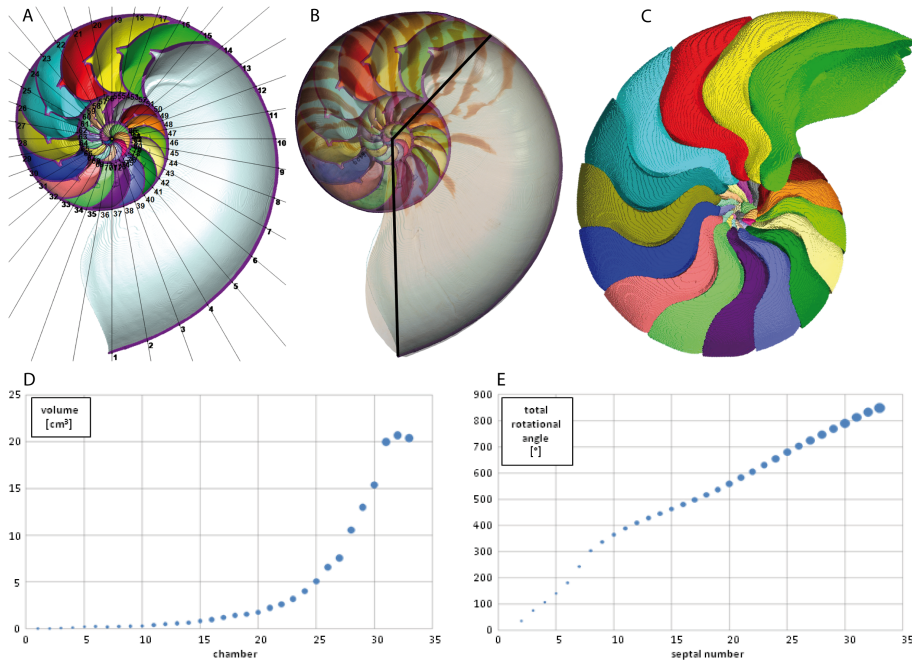


Fig. 6. *Nautilus pompilius* from the Philippines, 17 cm in diameter. **(A)** median section with a 10° grid and markers necessary for the description of the conch morphology like diameter (dm), umbilical width (uw) or whorl height (wh); **(B)** transparent photography of the shell, overlying the image of **(A)**, the two black bars document the body chamber length which is 136°; **(C)** phragmocone without body chamber and shell material, same orientation as in **(A)** and **(B)**; **(D)** and **(E)** ontogenetic trajectories of different conch parameters with: **(D)** chamber volume in cm³ which is important for the buoyancy calculation; **(E)** total rotational angle as indicator for continuously, in- or decreasing septal spacing. Increasing size of the blue dots represents ontogeny.

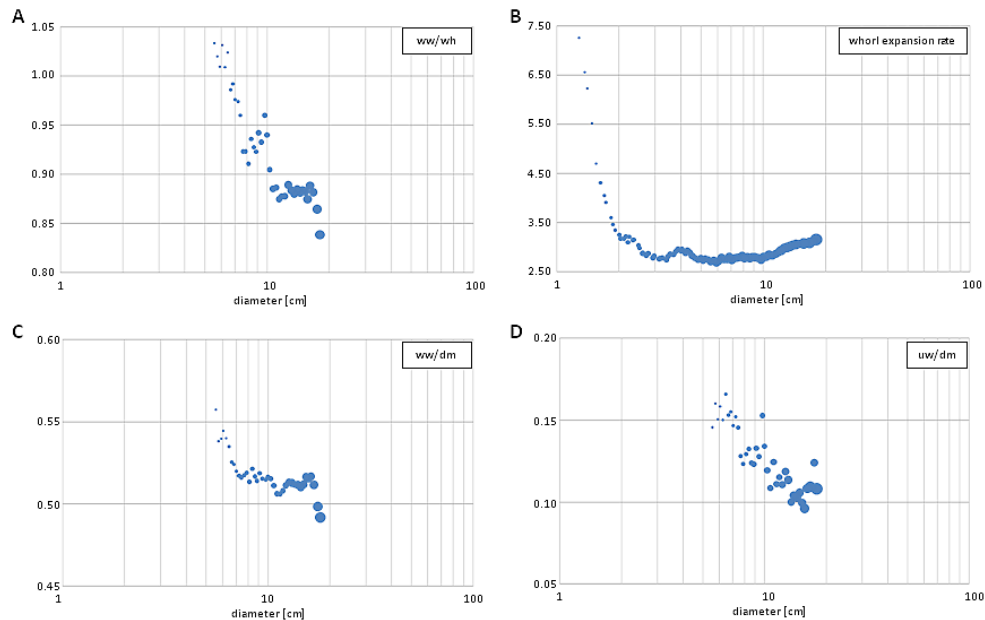


Fig. 7. *Nautilus pompilius* ontogenetic trajectories of different conch parameter for the same specimen shown in Fig. 6. According to Korn (2010) main conch features are: diameter (dm), umbilical width (uw), whorl height (wh), and whorl width (ww) and for heteromorph ammonoids the whorl interspace (wi) as well. Ratios derived from primary data (e.g., UWI, CWI, WWI and WER) can be plotted for comparison in a logarithmic plot against conch diameter. **(A)** Whorl width index (ww/wh); **(B)** Whorl expansion rate (WER); **(C)** Conch width index (ww/dm); **(D)** Umbilical width index (uw/dm). Increasing size of the blue dots represents ontogeny.

[Title Page](#)
[Abstract](#)
[Introduction](#)
[Conclusions](#)
[References](#)
[Tables](#)
[Figures](#)
[◀](#)
[▶](#)
[◀](#)
[▶](#)
[Back](#)
[Close](#)
[Full Screen / Esc](#)
[Printer-friendly Version](#)
[Interactive Discussion](#)


BGD

10, 18803–18851, 2013

Non-invasive imaging methods in cephalopod research

R. Hoffmann et al.

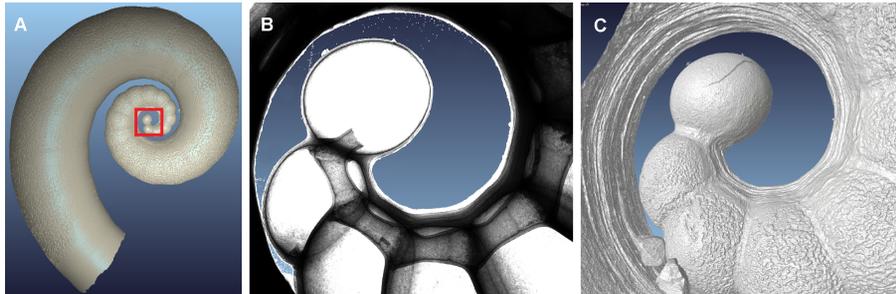


Fig. 8. Nano-CT scan (res. 1.8 μm) of *Spirula spirula* from the Canary Island (1.6 cm in diameter). **(A)** (isosurface) showing the distribution of the reticulate pattern, which is not present at the aperture and the ventral area. Red box encloses the earliest chamber built within the egg (protoconch). **(B)** X-ray rendering, close up of **(A)** with the protoconch and the organic strand (siphuncle) that connects all chambers of the shell; **(C)** surface rendering of the same area as in **(B)**, surface view with the reticulate pattern and the ventral area of the first whorl with growth lines of the “ventral rib” pointing to the solid base of the organic membrane (compare Warnke and Boletzky, 2009).

Title Page

Abstract

Introduction

Conclusions

References

Tables

Figures

◀

▶

◀

▶

Back

Close

Full Screen / Esc

Printer-friendly Version

Interactive Discussion



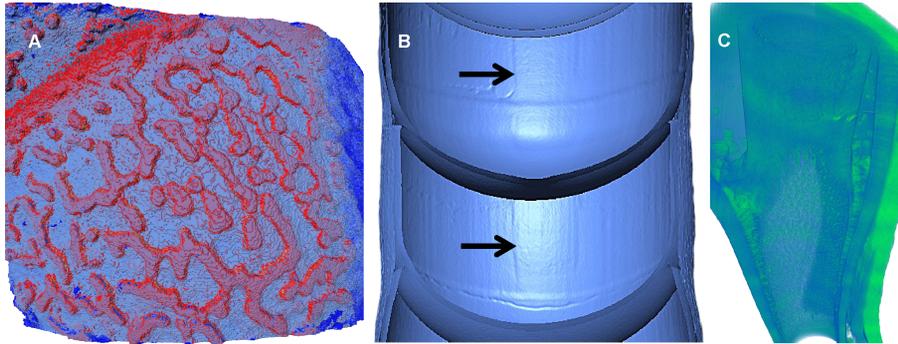


Fig. 9. The same *Spirula spirula* specimen as in Fig. 8. **(A)** close up of the reticulate surface pattern (nano-CT res. $1.8\ \mu\text{m}$); **(B)** nano-CT image (res. $1.8\ \mu\text{m}$) of the inner surface of two successive chambers showing a rectangular dorsal attachment scar (arrows); **(C)** SR μ CT image (res. $0.74\ \mu\text{m}$) of the siphuncle and ventral part of the shell, showing the light green pillar zone all along the calcareous tube in the lower half of the image, orientation of the image with the top in grow direction.

Title Page

Abstract

Introduction

Conclusions

References

Tables

Figures

◀

▶

◀

▶

Back

Close

Full Screen / Esc

Printer-friendly Version

Interactive Discussion



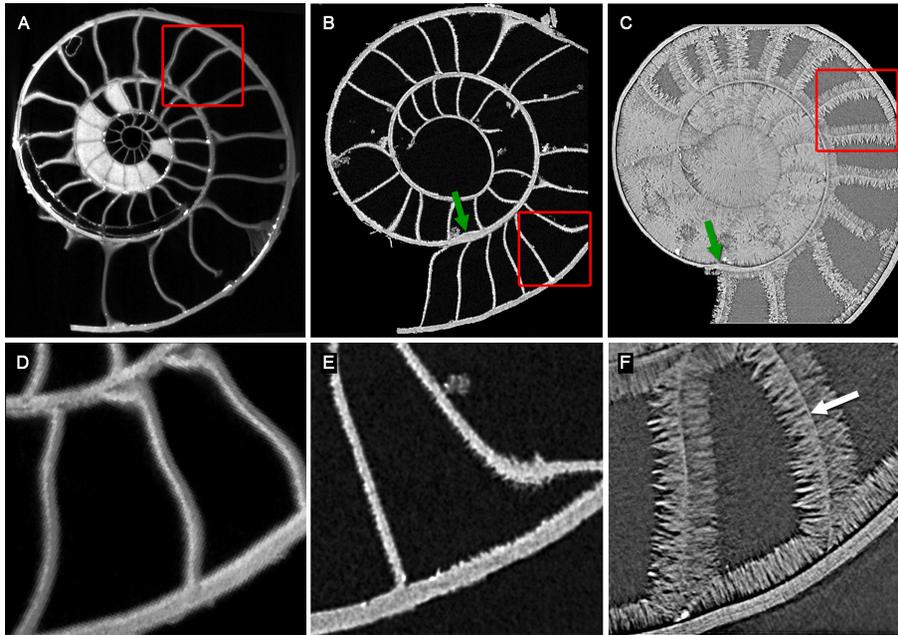


Fig. 10. Three juvenile *Cadoceras* sp. specimens from the Upper Jurassic (Callovian) of Russia. **(A and D)** micro-CT scan with a resolution of $7.5\ \mu\text{m}$; **(D)** close up of **(A)** (red box), the original shell material cannot be distinguished from secondary calcite crystals that cover the inner surface of the conch wall and septa; **(B and E)** nano-CT scan with a resolution of $1.0\ \mu\text{m}$; **(B)** nepionic constriction indicated by green arrow; **(E)** close up of **(B)** (red box), some secondary calcite crystals become visible and the former smooth appearing surface turns into a rough one; **(C and F)** SR μ CT with a resolution of $0.74\ \mu\text{m}$; **(C)** nepionic constriction indicated by green arrow; **(F)** close up of **(C)** (red box), this specimen shows a rather heavy infill with secondary calcite crystals, however the original shell (e.g., thin septa) is distinguishable (white arrow).

BGD

10, 18803–18851, 2013

Non-invasive imaging methods in cephalopod research

R. Hoffmann et al.

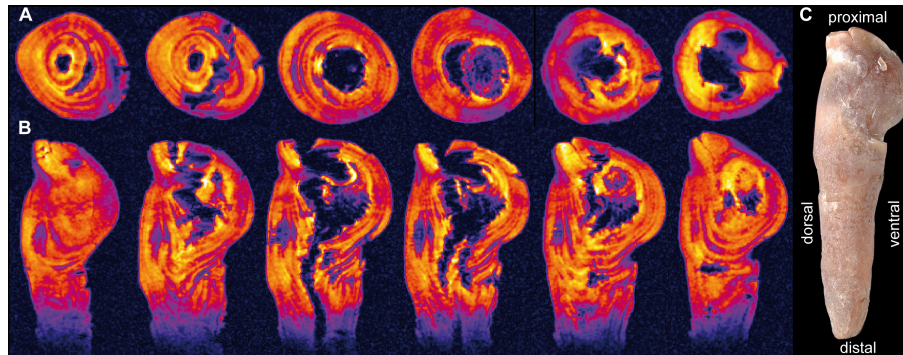


Fig. 11. *Hibolites jaculoides* from the Lower Cretaceous (Hauterivian) of Northwestern Germany (PB251 Coll. H. Keupp; 4.2 cm long). This specimen shows a pathology due to a parasite encapsulated within the shell secreting mantle epithelia during early ontogeny. **(A)** Images of an MRI scan of the cross section from distal to proximal (left dorsal, right ventral); **(B)** Images of the same MRI scan of the longitudinal section (same orientation as in **C**), rows **(A and B)** are showing the internal malformation of the rostral skeleton; **(C)** Specimen in lateral view. (Modified from Mietchen et al., 2005.)

Title Page

Abstract

Introduction

Conclusions

References

Tables

Figures

◀

▶

◀

▶

Back

Close

Full Screen / Esc

Printer-friendly Version

Interactive Discussion



Non-invasive imaging methods in cephalopod research

R. Hoffmann et al.

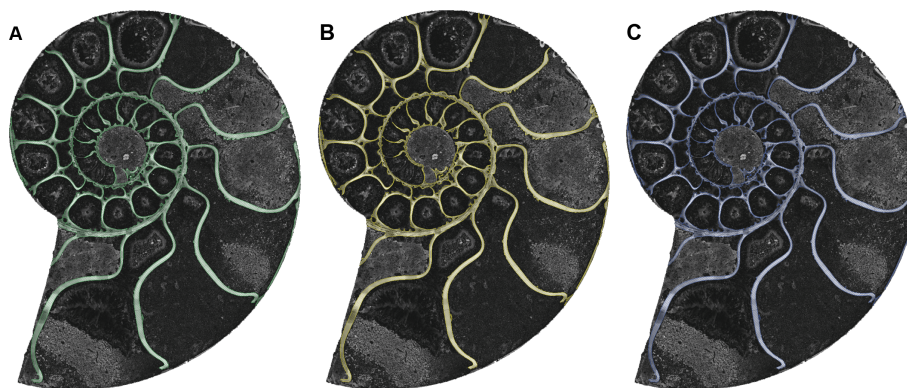


Fig. 12. 2-D-scan image of a cut and polished *Argonauticeras* sp. along the median plane. From the Lower Cretaceous (Albian) of Madagascar (diameter = 9.5 cm). **(A)** “growth model” – selected shell material in green with one pixel added to the complete outline seen in **(B)**; **(B)** selected shell material in yellow obtained after the application of a manually chosen threshold for selection; **(C)** “shrink model” – selected shell material in blue with one pixel subtracted from the complete outline seen in **(B)**, pixel size for a 600 dpi scan = $42.3\ \mu\text{m}$, difference from **(A)** to **(B)** and **(B)** to **(C)** = 9.5% cp. with Fig. 5 for the PVE, note that the “voxel size” obtained is not isotropic due to differing distances between each slice and even in the “growth model” **(A)** not all shell material was selected due to low grey values, an error of about 20% for a volume calculation (shell or chambers) is suspected.

Title Page

Abstract

Introduction

Conclusions

References

Tables

Figures

◀

▶

◀

▶

Back

Close

Full Screen / Esc

Printer-friendly Version

Interactive Discussion

